

How do the LIGO-Virgo-KAGRA's Heavy Black Holes Form? No evidence for core-collapse Intermediate-mass black holes in GWTC-4

FAN-XIAO-YU XIA (夏凡小雨) ¹, YUAN-ZHU WANG (王远瞩) ² AND YING QIN (秦颖) ³

¹Key Laboratory of Dark Matter and Space Astronomy, Purple Mountain Observatory, Chinese Academy of Sciences, Nanjing 210023, People's Republic of China

²Institute for Theoretical Physics and Cosmology, Zhejiang University of Technology, Hangzhou, 310032, People's Republic of China

³Department of Physics, Anhui Normal University, Wuhu, Anhui 241000, People's Republic of China

ABSTRACT

We investigate the population properties of binary black holes (BBHs) from the LIGOVirgoKAGRA collaboration, focusing especially on those in the high-mass range, using the newly released GWTC-4 catalog. For the first time, we search for a subpopulation of low-spin intermediate-mass black holes (IMBHs) that would indicate formation via stellar core collapse. With the currently available catalog, we find no evidence for such a subpopulation, and set a 90% upper limit on the merger rate of collapse-formed IMBHs at $0.077 \text{ Gpc}^{-3} \text{ yr}^{-1}$. The mass distribution of low-spin (stellar-origin) black holes truncates at $65^{+23}_{-22} M_{\odot}$, consistent with the lower edge of the pair-instability mass gap (PIMG), although we cannot directly determine its upper boundary from current data. Informed by stellar evolution theory, we estimate the upper edge of the PIMG to be $150 \pm 24 M_{\odot}$. We find that the observed IMBHs belong to a high-spin subpopulation, consistent with formation through successive hierarchical mergers.

Keywords: Binary Black Holes; Gravitational Waves; Stellar Evolution; Active Galactic Nuclei

1. INTRODUCTION

LIGO, Virgo, and KAGRA (LIGO Scientific Collaboration et al. 2015; Acernese et al. 2015; Aso et al. 2013) have detected more than 300 gravitational-wave (GW) signals from binary black hole (BBH) mergers in the first four observing runs (see *GraceDB*), which have contributed to fundamental Physics and Cosmology (Abbott et al. 2017; Wang et al. 2025a; Abac et al. 2025b,c; Tang et al. 2026). A significant fraction of BBHs have unexpectedly large masses, challenging stellar evolution theories (Abbott et al. 2021, 2023a; The LIGO Scientific Collaboration et al. 2025b).

Intermediate-mass black holes (IMBHs, Miller & Colbert 2004), with masses ranging from $\sim 10^2$ to $10^5 M_{\odot}$, have previously been observed as remnants of BBH mergers (e.g., GW190521 Abbott et al. 2020a). Recent observations show that some IMBHs are also merging with other BHs (e.g., GW231123 The LIGO Scientific Collaboration et al. 2025a).

These unexpected events have sparked discussion regarding the origin and evolution of IMBHs in BBH systems (e.g., Stegmann et al. 2025a; Li et al. 2025b; Yuan et al. 2025; De Luca et al. 2025; Croon et al. 2025; Bartos & Haiman 2025; Popa & de Mink 2025a; Kiroğlu et al. 2025; Goyal et al. 2025; Paiella et al. 2025).

Stellar evolution models predict an upper mass cutoff of $\sim 40\text{--}65 M_{\odot}$ for BHs formed via core collapse, owing to (pulsational) pair-instability supernovae ((P)PISN, Fowler & Hoyle 1964; Barkat et al. 1967; Woosley 2017; Woosley & Heger 2021). More massive BBHs are therefore expected to form predominantly through hierarchical mergers of stellar-mass BHs in dense environments (Gerosa & Fishbach 2021). Alternatively, the direct collapse of very massive stars—such as Population III stars with helium core masses $\gtrsim 135 M_{\odot}$ —may also produce IMBHs and contribute to the observed BBH population (e.g., Marchant et al. 2016).

While individual, unusual events may offer clues to BBH formation channels (e.g., Abbott et al. 2020b,c,a; Abac et al. 2024; The LIGO Scientific Collaboration et al. 2025a), population-level analyses provide a more systematic avenue to identify BBH subpopulations

and their corresponding evolutionary pathways (Abbott et al. 2019, 2021, 2023b). Different formation channels are expected to imprint characteristic signatures on the BBH population—particularly in component masses and spins—allowing them to be statistically disentangled.

The detection of GW231123 is particularly intriguing, as the system likely contains one component beyond the pair-instability mass gap (PIMG) (The LIGO Scientific Collaboration et al. 2025a). However, the unusually large spin magnitudes inferred for this event suggest that both components are likely remnants of previous BBH mergers rather than first-generation BHs (Li et al. 2025b; Stegmann et al. 2025b; Li & Fan 2025). Motivated by this event and the full GWTC-4 catalog, we aim to determine whether any evidence exists for IMBH mergers formed via direct stellar core collapse.

Previous population studies indicate that BBHs with component masses above $\sim 45 M_{\odot}$ are broadly consistent with hierarchical merger origins (Wang et al. 2022; Li et al. 2024c,a, 2025c; Guo et al. 2024; Antonini et al. 2025b; Banagiri et al. 2025; Tong et al. 2025b; Plunkett et al. 2026; Guttman et al. 2026; Passenger et al. 2025). While Wang et al. (2025b) showed that the maximum-mass cutoff for the low-spin subpopulation may extend up to $\sim 65 M_{\odot}$. These findings naturally raise several further questions: Are any high-mass BBH events (e.g., those containing IMBH components) formed via stellar collapse? How massive can IMBHs become through hierarchical mergers? And where is the far-side edge of the PISN mass gap, if it exists?

Although recent GWTC-4 population analyses suggest that high-mass events are consistent with hierarchical mergers (Antonini et al. 2025a; Banagiri et al. 2025; Li et al. 2025d; Wang et al. 2025b; Tong et al. 2025a), these studies typically model only two broad subpopulations, making it difficult to identify a distinct low-spin population within or beyond the PIMG. Since low-spin events are unlikely to arise from hierarchical mergers (Fishbach et al. 2017; Gerosa & Berti 2017; Gerosa & Fishbach 2021), the detection of such a subpopulation—if present—would provide important insights into primordial BHs or collapse-formed IMBHs. In this work, we therefore perform a dedicated population analysis of GWTC-4 aimed at searching for such a population. Additionally, we also aim to characterize the shape of the expected PIMG.

2. METHODS

We perform a population analysis of the BBHs in GWTC-4, employing hierarchical Bayesian inference to estimate the hyperparameters of the population model; see Appendix A for details. Following The LIGO Sci-

entific Collaboration et al. (2025b), we select 153 BBH events with a false alarm rate (FAR) $< 1 \text{ yr}^{-1}$ for our analysis. Posterior samples for these events are obtained from `events-zenodo` (Collaboration et al. 2025).

2.1. spin versus mass model (Main Model)

The spin magnitudes of black holes are among the key observables for determining their origins (Mandel & Farmer 2022). First-generation (core-collapse) BHs and primordial BHs are expected to be either slowly spinning (Fuller & Ma 2019; Chiba & Yokoyama 2017) or to possess moderate spins acquired through tidal spin-up (e.g. Qin et al. 2018; Marchant et al. 2016; Bavera et al. 2020; Wang et al. 2026) or accretion (e.g. Shao & Li 2022; Mandel & Farmer 2022) (although see e.g. Croon et al. (2025); Kiroğlu et al. (2025); Popa & de Mink (2025b); Bartos & Haiman (2025) for alternative views). Higher-generation BHs, in contrast, are expected to be highly spinning, with spin magnitudes that typically peak at ~ 0.7 (Gerosa & Berti 2017; Fishbach et al. 2017; Gerosa & Fishbach 2021) or even larger values due to gas hardening in AGN disks (Vaccaro et al. 2024). In this work, we therefore construct a population model designed to identify the subpopulations of higher-generation and first-generation BHs mainly based on their spin magnitudes.

We adopt the population model of Li et al. (2024c), in which the joint distribution of component mass m and spin magnitude χ is described by a two-component mixture:

$$\pi(m, \chi | \Lambda) = \pi_1(m, \chi | \Lambda_1) (1 - r_2) + \pi_2(m, \chi | \Lambda_2) r_2, \quad (1)$$

where each subpopulation factorizes into independent mass and spin distributions,

$$\pi_i(m, \chi | \Lambda_i) = P_{m,i}(m | \Lambda_i) P_{\chi,i}(\chi | \Lambda_i). \quad (2)$$

The spin distribution $P_{\chi,i}(\chi | \Lambda_i)$ is modeled as a Gaussian $\mathcal{G}_{[\chi_{\min,i}, \chi_{\max,i}]}(\chi | \mu_{\chi,i}, \sigma_{\chi,i})$ truncated to the interval $[\chi_{\min,i}, \chi_{\max,i}]$. For the second subpopulation, the mass function is given by a PowerLaw+Spline model \mathcal{PS} (Edelman et al. 2022); see Appendix 2.2 for its definition. In this work, we extend the mass function of the first subpopulation to allow for a potential contribution from collapse-formed IMBHs beyond the pair-instability mass gap. Specifically, we set

$$P_{m,1}(m | \Lambda_1) = \mathcal{PS}(m | \Lambda_1) (1 - r_{\mathcal{LM}}) + \mathcal{PL}(m | \alpha_{\mathcal{LM}}, m_{\min, \mathcal{LM}}, m_{\max, \mathcal{LM}}) r_{\mathcal{LM}}, \quad (3)$$

where \mathcal{PL} is a truncated power-law distribution (Abbott et al. 2021), designed to capture the possible low-spin IMBH population formed via stellar collapse.

The overall population model is

$$\begin{aligned} \pi(\lambda|\Lambda) \propto & \pi(m_1, \chi_1, |\Lambda) \pi(m_2, \chi_2, |\Lambda) \mathcal{F}_{\text{pair}}(m_1, m_2|\beta) \\ & \times \mathcal{GU}(\cos \theta_1, \cos \theta_2|\zeta, \mu_t, \sigma_t) P_z(z|\gamma), \end{aligned} \quad (4)$$

where $\mathcal{F}_{\text{pair}}(m_1, m_2|\beta) = (m_2/m_1)^\beta$ is the pairing function, $\mathcal{GU}(\cos \theta_1, \cos \theta_2|\zeta, \mu_t, \sigma_t) = (1 - \zeta)U(\cos \theta_1, \cos \theta_2| - 1, 1) + \zeta\mathcal{G}_{[-1,1]}(\cos \theta_1, \cos \theta_2|\mu_t, \sigma_t)$ is for spin orientation distribution, which is the mixture of isotropic and nearly aligned assemblies. $P_z(z|\gamma)$ is for the redshift distribution, where we assume the merger rate density evolving with redshift as $R(z) = R_0(1+z)^\gamma$, and R_0 is the local merger rate.

2.2. model under stellar evolution theories (Alternative Model)

Since we find no evidence for a low-spin IMBH population (as presented in Section 3), the upper edge of the PIMG cannot be directly determined. We therefore adopt an alternative model in which the far-side edge is inferred under the guidance of stellar evolution theory, assuming that the low-spin subpopulation's cutoff defines the lower edge of the gap. In this model, we adopt a gap width of $80 \pm 8 M_\odot$ based on simulations (Farmer et al. 2020), which found the width to remain approximately constant at $83_{-8}^{+5} M_\odot$, while the individual lower and upper edges are only weakly constrained. The theoretically motivated mass function is then written as

$$P_{m,1}(m|\Lambda_1) \propto \mathcal{PS}(m|\Lambda_1) f_{\text{Gap}}(m|g_{\text{low}}, g_{\text{wide}}), \quad (5)$$

with

$$f(m|g_{\text{low}}, g_{\text{wide}}) = \begin{cases} 1, & \text{for } m < g_{\text{low}}, \\ 0, & \text{for } g_{\text{low}} < m < g_{\text{low}} + g_{\text{wide}}, \\ 1, & \text{for } m > g_{\text{low}} + g_{\text{wide}} \end{cases} \quad (6)$$

2.3. mass-only model

Even if the mass range of the PIMG in the first-generation black hole mass function is partly filled by higher-generation black holes from hierarchical mergers, a corresponding dip or deficit may still be imprinted on the overall binary black hole mass distribution. To search for this potential PIMG signature using mass information alone, we construct a population model that does not incorporate spin parameters. The parameterised joint mass distribution is given by

$$\pi(m_1, m_2|\Lambda) \propto P(m_1|\Lambda) P(m_2|\Lambda) (m_2/m_1)^\beta F_{\text{gap}}(m_1, m_2|\Lambda), \quad (7)$$

where $P(m|\Lambda)$ is the underlying (pre-pairing) mass function adopted for both component masses; here we use

the POWERLAW + 2 PEAK parametrisation introduced in The LIGO Scientific Collaboration et al. (2025b). The factor $F_{\text{gap}}(m_1, m_2|\Lambda)$ describes the location of a possible gap or dip in the mass function of the secondary component (or of both components).

We consider three parametrisations of the gap/dip factor F_{gap} . The function f_{gap} describing a dip or gap in the mass distribution of a single component is defined as

$$f_{\text{gap}}(m|g_{\text{low}}, g_{\text{up}}, A) = \begin{cases} 1, & \text{for } m < g_{\text{low}}, \\ 1 - A, & \text{for } g_{\text{low}} < m < g_{\text{up}}, \\ 1, & \text{for } m > g_{\text{up}}, \end{cases} \quad (8)$$

where g_{low} and g_{up} mark the edges of the underlying gap or dip, and $A \in [0, 1]$ controls the depth ($A = 1$ corresponds to a completely empty gap; see Fishbach et al. (2020)). The three cases are then specified as follows.

- **Case 1: Dip in both primary and secondary masses.**

$$\begin{aligned} F_{\text{gap}}(m_1, m_2|\Lambda) = \\ f_{\text{gap}}(m_1|g_{\text{low}}, g_{\text{up}}, A) f_{\text{gap}}(m_2|g_{\text{low}}, g_{\text{up}}, A). \end{aligned} \quad (9)$$

- **Case 2: Dip only in the secondary mass.**

$$\begin{aligned} F_{\text{gap}}(m_1, m_2|\Lambda) = \\ f_{\text{gap}}(m_1|g_{\text{low}}, g_{\text{up}}, A=0) f_{\text{gap}}(m_2|g_{\text{low}}, g_{\text{up}}, A). \end{aligned} \quad (10)$$

- **Case 3: Gap in the secondary mass function.**

$$\begin{aligned} F_{\text{gap}}(m_1, m_2|\Lambda) = \\ f_{\text{gap}}(m_1|g_{\text{low}}, g_{\text{up}}, A=0) f_{\text{gap}}(m_2|g_{\text{low}}, g_{\text{up}}, A=1). \end{aligned} \quad (11)$$

For all cases, the merger rate density evolution model is the same as in the main model introduced above.

3. RESULTS

In this Section we display the results inferred with our main model, alternative model, as well as the mass-only model introduced in Section 2.

3.1. No evidence for low-spin IMBHs

Figures 1 and 2 show the mass and spin distributions of the BBH population inferred with our main model. Two distinct subpopulations are clearly identified in both the primary and secondary black holes, indicated by the blue and orange curves.

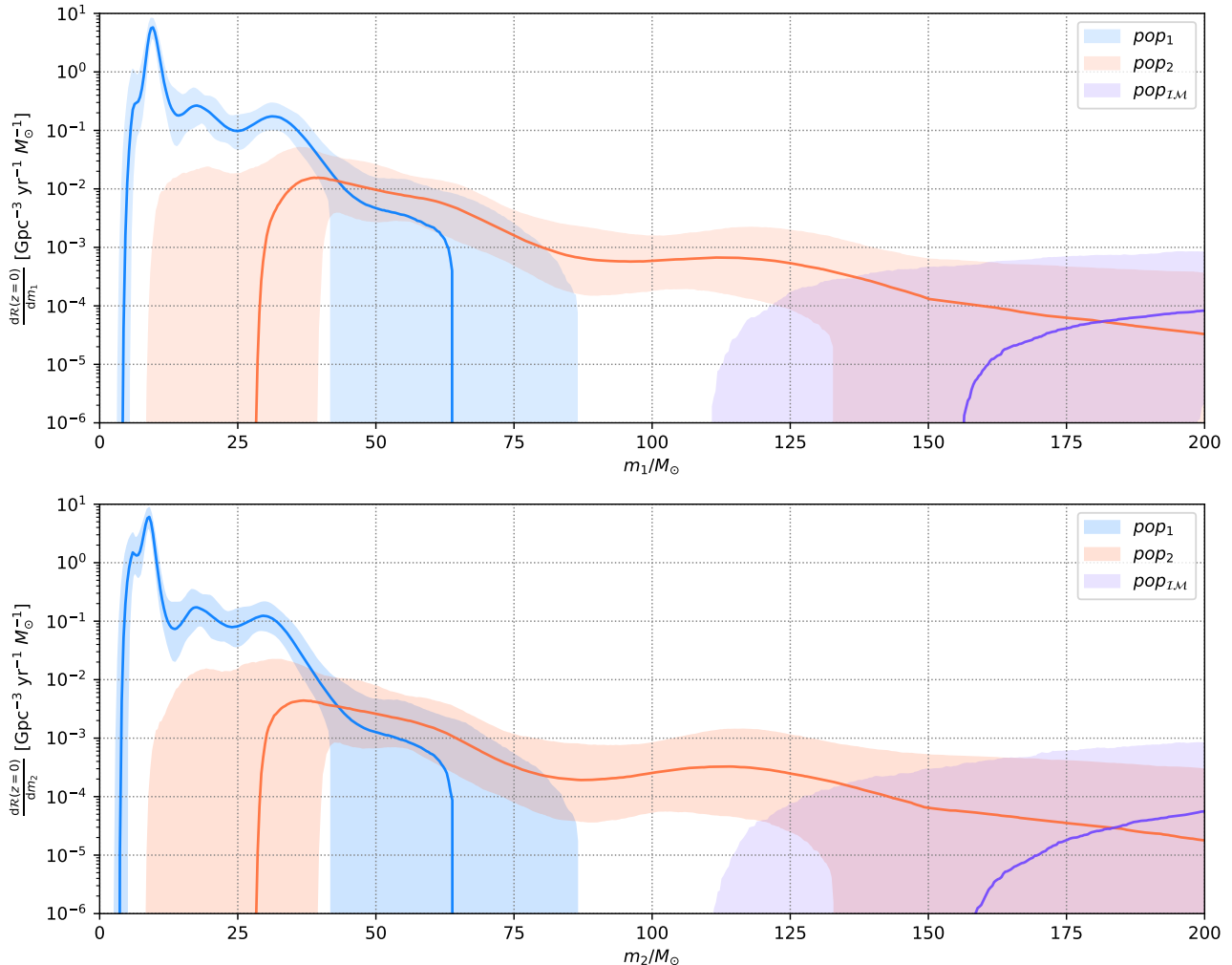


Figure 1. Component mass distributions of the primary (top) and secondary (bottom) black holes for the three subpopulations inferred with the Main Model. The solid curves are the medians and the shaded regions are for the 90% credible intervals.

The first subpopulation, referred to as the low-spin group, is characterized by small dimensionless spin magnitudes ($\chi \lesssim 0.3$), peaking at $\chi \sim 0.15$. Its mass distribution is confined to the lower-mass range ($\sim 5\text{--}65 M_\odot$) and exhibits a pronounced cutoff above $65^{+23}_{-22} M_\odot$. This behaviour is consistent with the expectations for black holes formed through stellar core collapse and the upper mass limit imposed by (pulsational) pair-instability processes (Farmer et al. 2019, 2020; Mapelli et al. 2020).

In contrast, the second (high-spin) subpopulation shows significantly larger spin magnitudes ($\chi \gtrsim 0.6$), with a peak around $\chi \sim 0.8$. Its mass distribution is broad, extending from about $20 M_\odot$ up to $\sim 150 M_\odot$ and possibly beyond, in agreement with expectations for hierarchical merger products.

Crucially, we find no evidence for an additional low-spin, high-mass subpopulation above $100 M_\odot$, as the mixture fraction r_{IM} of the $\mathcal{P}\mathcal{L}$ component in

Eq. (3)—introduced to capture potential first-generation IMBHs—is consistent with zero. If we interpret the low-spin subpopulation as first-generation BHs, the 90% credibility upper limit on the local merger rate of collapse-formed IMBH mergers is $< 0.077 \text{ Gpc}^{-3} \text{ yr}^{-1}$, see Appendix B.

3.2. The far-side edge of mass gap

We find no evidence for a low-spin subpopulation with masses above $100 M_\odot$, which precludes a direct measurement of the PIMG’s upper edge. To address this, we employ the Alternative Model described in Section 2.3. Adopting a Gaussian prior on the PIMG width of $80 \pm 8 M_\odot$ (1σ) (Farmer et al. 2020), we indirectly constrain the upper edge to be $g_{\text{up}} = 150 \pm 24 M_\odot$ (see Figure 5 in the Appendix).

We therefore analyze the PIMG using the mass-only model (Section 2.3). This approach is motivated by

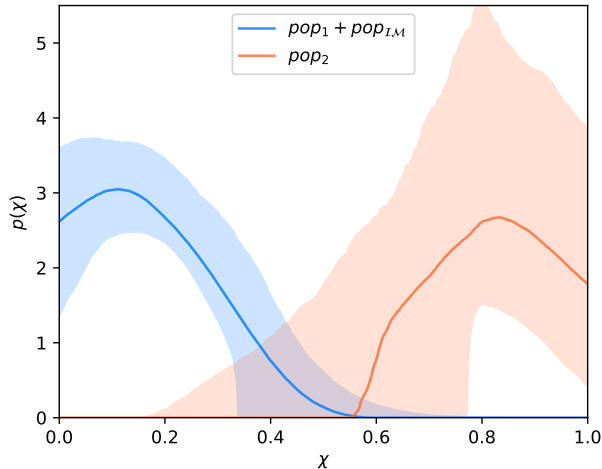


Figure 2. Distribution of spin magnitudes of black holes for the subpopulations inferred with the Main Model. The solid curves are the medians and the shaded regions are for the 90% credible intervals.

the expectation that if core-collapse IMBHs are significantly more abundant than those formed via hierarchical mergers, a distinct signature of the PIMG’s upper edge should be imprinted on the mass function. Figure 3 shows the inferred primary and secondary mass distributions for the three cases. In the primary mass distribution, we find no evidence for a pronounced dip or gap, with all models yielding nearly identical results. This consistency suggests that hierarchical mergers are sufficiently frequent in the high-mass regime to largely erase the expected PIMG signature. Regarding the secondary mass distribution, we similarly find no statistically significant evidence for a dip or gap. While an entirely empty gap ($A = 1$) is mildly preferred over a completely filled one ($A = 0$), the depth of any potential dip remains weakly constrained (see Figure 6 in Appendix B).

For Case 3 (empty gap in the secondary-mass distribution), we obtain $g_{\text{low}} = 53_{-10}^{+23} M_{\odot}$ and $g_{\text{up}} = 111_{-9}^{+15} M_{\odot}$. The lower edge g_{low} is consistent with results from other parametric models (Tong et al. 2025b; Ray & Kalogera 2025) and agrees with $m_{\text{max},1}$ (i.e., g_{low}) in the Main (Alternative) Model. However, the upper edge g_{up} is notably lower than the value inferred from $g_{\text{low}} + g_{\text{wide}}$ in the Alternative Model (see Figure 4) and than theoretical expectations (Farmer et al. 2020), revealing some tension. We note that g_{up} is primarily driven by the secondary mass of GW231123, which likely accounts for this discrepancy.

3.3. The origin of LVK’s most massive black holes and their merger rate

Analysis of the Main Model indicates that both components of GW231123 belong to the high-spin subpopulation, consistent with a hierarchical merger scenario (Gerosa & Berti 2017; Fishbach et al. 2017; The LIGO Scientific Collaboration et al. 2025a). Moreover, their masses do not lie significantly beyond the theoretically expected upper edge of the PIMG obtained from the Alternative Model (Farmer et al. 2020) (Figure 4). Thus, GW231123 is most likely a binary composed of higher-generation black holes.

We further find that the maximum masses of both subpopulations remain essentially unconstrained. Theoretically, each could extend to $\gtrsim 300 M_{\odot}$, and the absence of such detections is likely due to the limited sensitivity of current detectors (LIGO Scientific Collaboration et al. 2015; Abbott et al. 2018). Accordingly, we place a model-dependent 90% credible upper limit on the merger rate density of IMBHs with $m_1 \gtrsim 150 M_{\odot}$: $d\mathcal{R}(z=0)/dm_1 \lesssim 10^{-4}\text{--}10^{-3} \text{ Gpc}^{-3} \text{ yr}^{-1} M_{\odot}^{-1}$ (see Figure 8). Detecting such systems will likely require next-generation observatories (Amaro-Seoane et al. 2023; Li et al. 2025a; Abac et al. 2025a).

4. CONCLUSIONS AND DISCUSSION

We conducted population analysis of binary black holes in GWTC-4, focusing on their component masses and spins to investigate the origin of massive black holes (within or beyond the expected PIMG). Our main findings are:

1. **No evidence for low-spin (stellar-collapse) IMBHs:** We find no significant evidence for a subpopulation of low-spin IMBHs that would be indicative of formation via direct stellar core collapse. The mixture fraction for such a potential population is constrained to < 0.017 (90% credibility). This places an upper limit on the local merger rate of collapse-formed IMBHs at $0.077 \text{ Gpc}^{-3} \text{ yr}^{-1}$.
2. **Constraints on the PISN mass gap (PIMG):** The mass distribution of the identified low-spin subpopulation, consistent with first-generation stellar-origin BHs, shows a truncation. We constrain the *lower* edge of the pair-instability mass gap to $\sim 65 M_{\odot}$, though find no statistically significant evidence in the current data to determine the *upper* boundary of the PIMG. There may be a gap with *upper* edge (of $111_{-9}^{+15} M_{\odot}$) in the secondary-mass distribution, which, however, may not be the PIMG. If we assume the width of PIMG to be $80 \pm 8 M_{\odot}$ as predicted by Farmer et al. (2020), we find the *upper* edge to be $150 \pm 24 M_{\odot}$.

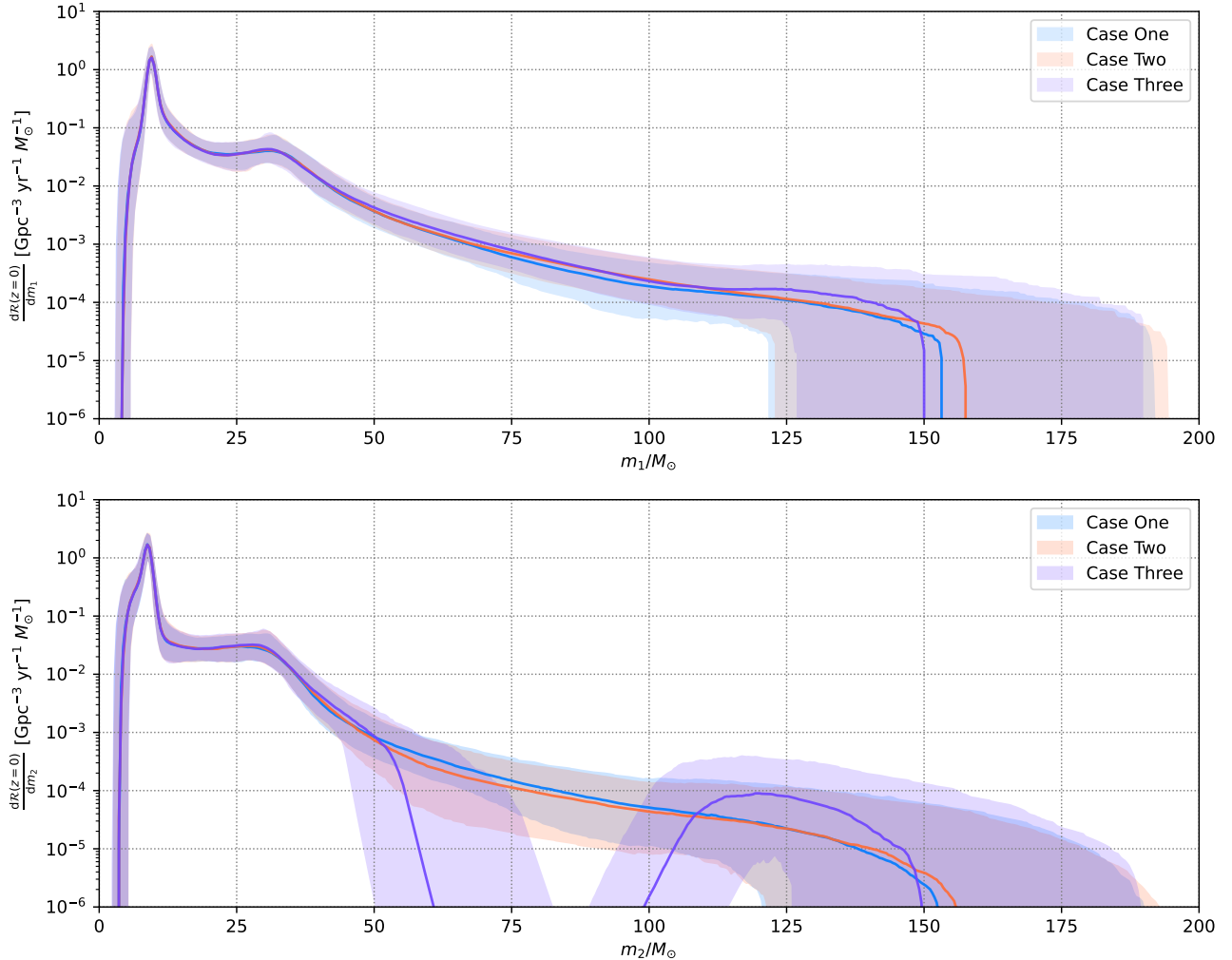


Figure 3. Mass distributions of the primary (a) and secondary (b) black holes inferred with the mass-only model for three cases. The solid curves are the medians and the shaded regions are for the 90% credible intervals.

3. Hierarchical merger origin for the most massive BHs: The IMBHs observed (e.g., in GW231123) belong to the high-spin ($\chi \gtrsim 0.6$) subpopulation. Their spin and mass distributions are consistent with expectations for BHs formed through successive hierarchical mergers in dense environments, like globular clusters or AGN disks.

While hierarchical mergers in dense environments remain the most consistent formation channel for the most massive BBHs in our findings, alternative origins for high-spin, high-mass black holes cannot be entirely excluded. For instance, Primordial Black Holes (PBHs) could acquire high spins through accretion (Yuan et al. 2025; De Luca et al. 2025), although their abundance and merger rates are still highly uncertain (Ali-Haïmoud et al. 2017; De Luca et al. 2020). Population III stars or chemically homogeneous evolution (CHE) at low metallicity can naturally produce rapidly rotating progeni-

tors and give rise to high-mass, high-spin BBHs such as GW231123 (Paiella et al. 2025; Popa & de Mink 2025a)¹. Stellar mergers or sustained accretion onto stellar-mass BHs (Renzo et al. 2020; Kiroğlu et al. 2025; Bartos & Haiman 2025) could also form massive, highly spinning BHs (but see Broekgaarden et al. (2022)). Direct collapse of a single rotating massive star can produce BHs resembling the component objects of GW231123 (Gottlieb et al. 2025; Croon et al. 2025; Baumgarte & Shapiro 2025). These alternative pathways make it difficult to distinguish hierarchical merger products from other formation scenarios using the currently available BBH catalog, which in turn prevents a clean, model-independent determination of the far-side edge of the

¹ Lensing and Overlapping effects may also produce GW231123-like events (Hu et al. 2025; Yang et al. 2025; Harshe et al. 2026, e.g.)

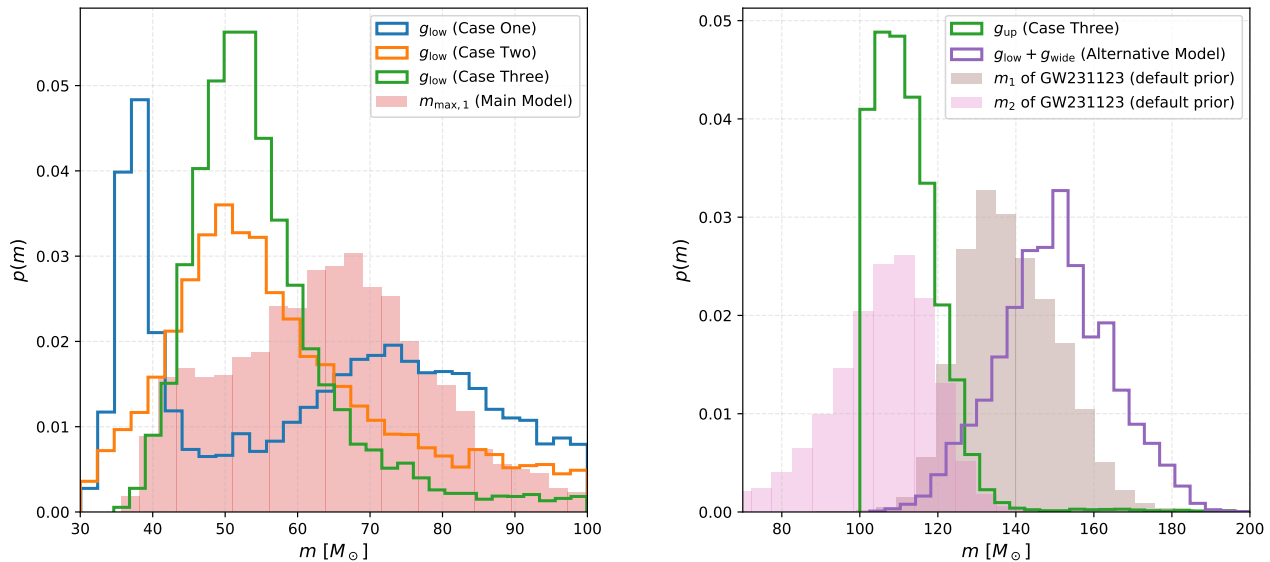


Figure 4. Left: The posterior distributions of maximum masses that are potentially associated to the lower edge of PIMG. Right: The posterior distributions of cutoff masses that are potentially associated to the upper edge of PIMG, compared to the component masses of GW231123.

PIMG from the existing population. Nevertheless, a clear observational diagnostic can break this degeneracy: the robust detection of even a single IMBH merger event with low spin would provide definitive evidence for IMBHs formed through stellar core collapse, thereby directly constraining the upper edge of the PIMG.

Ezquiaga & Holz (2021) demonstrated that the upper edge of the PIMG could, in principle, be constrained to the percent level with a few tens of events. However, a substantial population of hierarchical mergers in the relevant mass range may smear out this sharp cutoff, obscuring the mass boundary expected from stellar evolution. Such an effect has already been observed for the *lower* edge of the PIMG (Abbott et al. 2023a) and was addressed in previous work (Li et al. 2024c). Future low-frequency observatories such as LISA, TianQin, and Taiji (Luo et al. 2016; Amaro-Seoane et al. 2017; Hu & Wu 2017) will therefore be crucial: by detecting the slowly spinning IMBH binaries expected from core collapse, they could directly reveal this boundary (Sesana 2016; Moore et al. 2019).

Larger samples of detections, combined with more sophisticated population models that incorporate masses, spins, and redshifts, will be essential to disentangle the formation channels of the most massive binaries and to explore their potential role as seeds for supermassive black holes (King & Dehnen 2005). Furthermore, as distinct black hole subpopulations are identified, they will also contribute to cosmological studies through “spec-

tral sirens” or “multi-spectral sirens” (Farr et al. 2019; You et al. 2021; Li et al. 2024b). For instance, the core-collapse IMBH population – and thus the location of the PIMG’s upper edge – could provide novel constraints on cosmic expansion (Ezquiaga & Holz 2022).

Acknowledgments: We thank Yi-Zhong Fan, Shao-Peng Tang, and Yin-Jie Li for helpful suggestions. This work is supported by the National Natural Science Foundation of China (NSFC, No. 12303063 and No. 12203101). Y.Qin is supported by NSFC (No. 12473036 and No. 12573045) and Anhui Provincial Natural Science Foundation (No. 2308085MA29). This research has made use of data and software obtained from the Gravitational Wave Open Science Center (<https://www.gw-openscience.org>), a service of LIGO Laboratory, the LIGO Scientific Collaboration and the Virgo Collaboration. LIGO is funded by the U.S. National Science Foundation. Virgo is funded by the French Centre National de Recherche Scientifique (CNRS), the Italian Istituto Nazionale della Fisica Nucleare (INFN) and the Dutch Nikhef, with contributions by Polish and Hungarian institutes.

Software: Bilby (Ashton et al. 2019, version 1.1.4, ascl:1901.011, <https://git.ligo.org/lscsoft/bilby/>), PyMultiNest (Buchner 2016, version 2.11, ascl:1606.005, <https://github.com/JohannesBuchner/PyMultiNest>).

APPENDIX

A. HIERARCHICAL BAYESIAN INFERENCE

Following the framework of Mandel et al. (2019); Abbott et al. (2021, 2023a), given the population hyperparameters Λ , the likelihood of the GW data $\{d\}$ from N_{det} detections is

$$\mathcal{L}(\{d\}|\Lambda) \propto N^{N_{\text{det}}} e^{-N_{\text{exp}}} \prod_{i=1}^{N_{\text{det}}} \int \pi(\theta_i|\Lambda) \mathcal{L}(d_i|\theta_i) d\theta_i, \quad (\text{A1})$$

where $N = \int R(z|\Lambda) \frac{dV_c}{dz} \frac{T_{\text{obs}}}{1+z} dz$ is the total number of mergers occurring in the surveyed spacetime volume, and $N_{\text{exp}} = N \int P(\text{det}|\theta) \pi(\theta|\Lambda) d\theta$ is the expected number of detections, with $P(\text{det}|\theta)$ the detection probability. N_{exp} can be computed via a Monte Carlo integral over a reference set of injected signals², and the individual-event likelihood $\mathcal{L}(d_i|\theta_i)$ is evaluated using the available posterior samples; see the Appendix of Abbott et al. (2021) for details. Following The LIGO Scientific Collaboration et al. (2025b), the uncertainty of likelihood raising from the Monte Carlo integrals (Abbott et al. 2023a; Talbot & Golomb 2023) are controlled to be $\sigma_{\mathcal{L}}^2 < 1$.

B. ADDITIONAL RESULTS

Figure 5 shows the constraints on the PIMG features from the Alternative Model, namely g_{low} , g_{wide} , and the derived upper edge $g_{\text{up}} \equiv g_{\text{low}} + g_{\text{wide}}$. In this model we adopt a theoretically motivated prior on the PIMG width of $g_{\text{wide}} = 80 \pm 8 M_{\odot}$, based on the simulations of Farmer et al. (2020), which indicate that the PIMG width remains approximately constant at $83_{-8}^{+5} M_{\odot}$, while the lower edge is poorly constrained, varying between about 40 and 90 M_{\odot} . With this Alternative Model, we obtain $g_{\text{low}} = 68.8_{-22.1}^{+23.0} M_{\odot}$, consistent with the result from the Main Model, and the upper edge of the PIMG is constrained to be $g_{\text{up}} = 150.1 \pm 24.3 M_{\odot}$.

Table 3 gives the Bayes factors of the three mass-only model cases with respect to Case One, showing that all three are competitive. Figure 6 shows the posterior distributions; the inferred gap edges are broadly consistent across cases. For Case 3 (empty gap in the secondary-mass distribution), we obtain $g_{\text{low}} = 53_{-10}^{+23} M_{\odot}$ and $g_{\text{up}} = 111_{-9}^{+15} M_{\odot}$. The lower edge agrees with other parametric models (Tong et al. 2025b; Ray & Kalogera 2025), with $m_{\text{max},1}$ in the Main/Alternative Models, and with the drop in the primary-mass function observed in a previous catalog (Wang et al. 2021). The upper edge, however, is significantly lower than both the value from $g_{\text{low}} + g_{\text{wide}}$ in the Alternative Model (Figure 4) and theoretical expectations (Farmer et al. 2020), indicating tension.

Figure 7 shows the merger rate density inferred for the low-spin IMBH subpopulation under the Main Model, which is consistent with zero across the analyzed mass range, with a 90% upper limit of $0.077 \text{ Gpc}^{-3} \text{ yr}^{-1}$. Figure 8 displays the corresponding upper limits on the merger rate density for IMBHs from different subpopulations; we find the 90% credible upper limit on the merger rate density of IMBHs with $m_1 \gtrsim 150 M_{\odot}$ to be $d\mathcal{R}(z=0)/dm_1 \lesssim 10^{-4} \text{--} 10^{-3} \text{ Gpc}^{-3} \text{ yr}^{-1} M_{\odot}^{-1}$. Detecting such systems will likely require next-generation observatories (Amaro-Seoane et al. 2023; Li et al. 2025a; Abac et al. 2025a).

² Obtained from <https://zenodo.org/doi/10.5281/zenodo.5636815>.

Table 1. Summary of model parameters.

Parameter	Description	Prior
PowerLaw+Spline mass function		
$m_{\min,i}[M_{\odot}]$	The minimum mass	$U(2, 50)$
$m_{\max,1}[M_{\odot}] / m_{\max,2}[M_{\odot}]$	The maximum mass	$U(20, 100) / U(20, 500)$
α_i	Slope index of the power-law mass function	$U(-8, 8)$
$\delta_{m,i}[M_{\odot}]$	Smooth scale of the mass lower edge	$U(0, 10)$
$\{f_i^j\}_{j=2}^{11}$	Interpolation values of perturbation function	$\mathcal{N}(0, 1)$
r_2	mixture fraction for the second subpopulation	$U(0, 1)$
constraints		$m_{\min,i} < m_{\max,i}$
β_q	Slope index of the mass-ratio distribution	$U(-8, 8)$
Spin distribution		
$\chi_{\min,1} / \chi_{\min,2}$	Lower edge for χ distribution	$0 / U(0, 0.8)$
$\chi_{\max,1} / \chi_{\max,2}$	Upper edge for χ distribution	$U(0.2, 1) / 1$
$\mu_{\chi,i}$	Center values for χ distribution	$U(0, 1)$
$\sigma_{\chi,i}$	Width of the χ distribution	$U(0.05, 0.5)$
constraints		$\mu_{\chi,1} < \mu_{\chi,2}$
μ_t	peak of the $\cos \theta_{1,2}$ distribution for Gaussian	$U(0.1, 4)$
σ_t	width of the $\cos \theta_{1,2}$ distribution for Gaussian	$U(0.1, 4)$
ζ	the mixture fraction for Gaussian	$U(0, 1)$
Rate evolution model		
$\lg(R_0[\text{Gpc}^{-3} \text{ yr}^{-1}])$	Local merger rate density	$U(-3, 3)$
γ	Slope of the power-law	$U(-8, 8)$
Special for the Main Model		
		in the text
$m_{\min,\mathcal{IM}}[M_{\odot}]$	The minimum mass of stellar-formed IMBHs ($pop_{\mathcal{IM}}$)	$U(100, 150)$
$m_{\max,\mathcal{IM}}[M_{\odot}]$	The maximum mass for $pop_{\mathcal{IM}}$	$U(100, 500)$
$\alpha_{\mathcal{IM}}$	Slope index for $pop_{\mathcal{IM}}$	$U(-8, 8)$
$r_{\mathcal{IM}}$	Mixture fraction for $pop_{\mathcal{IM}}$ in the first subpopulation	$U(0, 1)$
constraints		$m_{\min,\mathcal{IM}} < m_{\max,\mathcal{IM}}$
Special for the Alternative Model		
$g_{\text{low}}[M_{\odot}]$	The lower edge of PIMG	$U(30, 100)$
$g_{\text{wide}}[M_{\odot}]$	The width of PIMG	$\mathcal{N}(80, 8)$

Note: U , $LogU$, \mathcal{N} are for Uniform, Log-Uniform, Normal distribution.

Table 2. Summary of parameters for mass-only model.

Parameter	Description	Prior
$m_{\min}[M_{\odot}]$	The minimum mass	$U(2, 10)$
$m_{\max}[M_{\odot}]$	The maximum mass	$U(100, 200)$
α	Slope index of the power-law mass function	$U(-8, 8)$
$\delta_m[M_{\odot}]$	Smooth scale of the mass lower edge	$U(0, 10)$
$\mu_1[M_{\odot}]$	Center value for the first peak	$U(5, 15)$
$\sigma_1[M_{\odot}]$	Width of the first peak	$U(1, 10)$
$\mu_2[M_{\odot}]$	Center value for the second peak	$U(15, 50)$
$\sigma_2[M_{\odot}]$	Width of the second peak	$U(1, 10)$
r_p	mixture fraction for the Gaussian peaks	$U(0, 1)$
r_2	mixture fraction of the second Gaussian peak	$U(0, 1)$
β_q	Slope index of the pairing function	$U(-8, 8)$
$g_{\text{low}}[M_{\odot}]$	The lower edge of PIMG	$U(30, 100)$
$g_{\text{up}}[M_{\odot}]$	The upper edge of PIMG	$\mathcal{N}(100, 200)$

Note: U , $\text{Log}U$, \mathcal{N} , \mathcal{G} are for Uniform, Log-Uniform, Normal distribution, and Gaussian distribution.

Table 3. Bayes factors for mass-only models relative to Case One

Cases for mass-only model	$\ln \mathcal{B}$
Case One	0
Case Two	0.4
Case Three	0.3

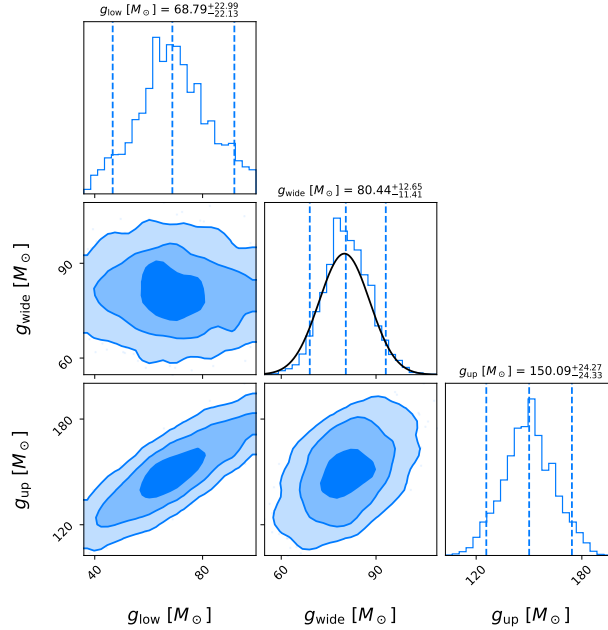


Figure 5. The posterior distributions of g_{low} , g_{wide} , and $g_{\text{up}} \equiv g_{\text{low}} + g_{\text{wide}}$ —which describe the edges and width of the PIMG—as obtained with the Alternative Model. The black curve indicates the prior on the PIMG width, taken to be $80 \pm 8 M_{\odot}$ following Farmer et al. (2020). The vertical lines indicate the median values and 90% credible intervals.

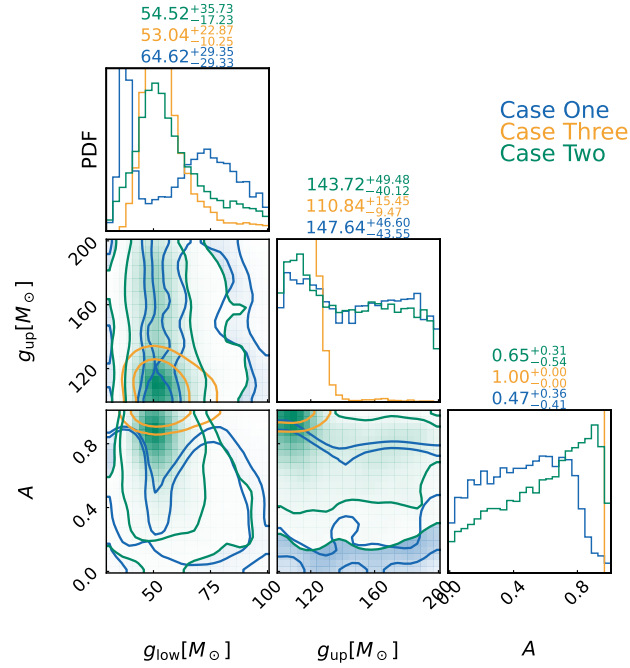


Figure 6. The posterior distribution of hyperparameters obtained with the mass-only models (Case One, Case Two, and Case Three). The values are for median and 90% credible intervals.

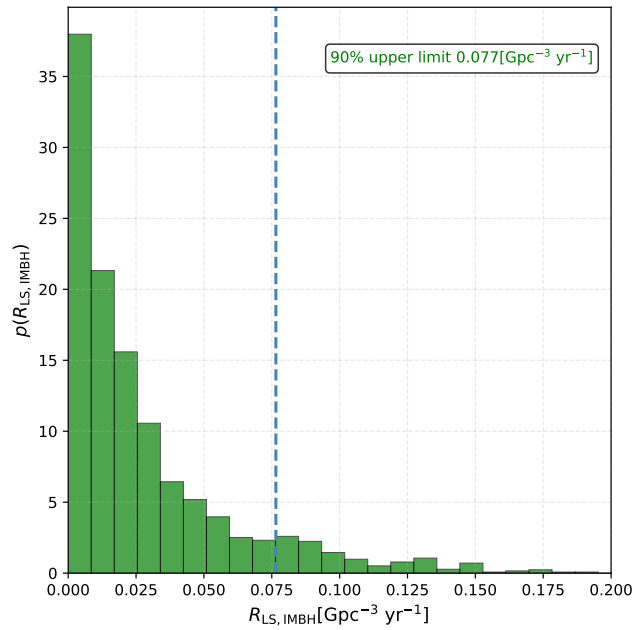


Figure 7. Merger rate of the low-spin IMBHs inferred with the Main Model. The vertical line indicate the 90% upper limit.

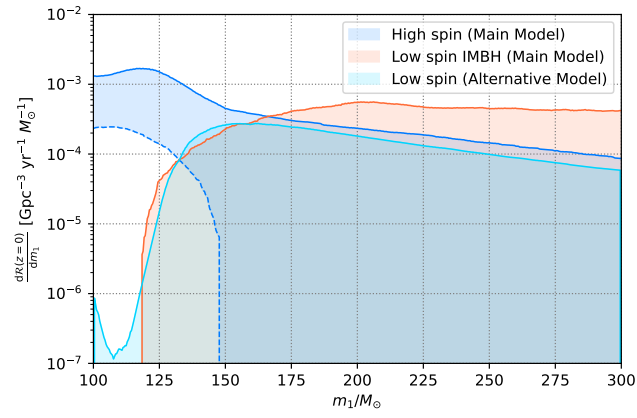


Figure 8. Upper limit (90%) of the IMBH mergers from different formation channels.

REFERENCES

- Abac, A., Abramo, R., Albanesi, S., et al. 2025a, arXiv e-prints, arXiv:2503.12263, doi: [10.48550/arXiv.2503.12263](https://doi.org/10.48550/arXiv.2503.12263)
- Abac, A. G., Abbott, R., Abouelfettouh, I., et al. 2024, *ApJL*, 970, L34, doi: [10.3847/2041-8213/ad5beb](https://doi.org/10.3847/2041-8213/ad5beb)
- Abac, A. G., Abouelfettouh, I., Acernese, F., et al. 2025b, *PhRvL*, 135, 111403, doi: [10.1103/kw5g-d732](https://doi.org/10.1103/kw5g-d732)
- . 2025c, *ApJL*, 993, L21, doi: [10.3847/2041-8213/ae0d54](https://doi.org/10.3847/2041-8213/ae0d54)
- Abbott, B. P., Abbott, R., Abbott, T. D., et al. 2017, *Nature*, 551, 85, doi: [10.1038/nature24471](https://doi.org/10.1038/nature24471)
- . 2018, *Living Reviews in Relativity*, 21, 3, doi: [10.1007/s41114-018-0012-9](https://doi.org/10.1007/s41114-018-0012-9)
- . 2019, *ApJL*, 882, L24, doi: [10.3847/2041-8213/ab3800](https://doi.org/10.3847/2041-8213/ab3800)
- Abbott, R., Abbott, T. D., Abraham, S., et al. 2020a, *PhRvL*, 125, 101102, doi: [10.1103/PhysRevLett.125.101102](https://doi.org/10.1103/PhysRevLett.125.101102)
- . 2020b, *PhRvD*, 102, 043015, doi: [10.1103/PhysRevD.102.043015](https://doi.org/10.1103/PhysRevD.102.043015)
- . 2020c, *ApJL*, 896, L44, doi: [10.3847/2041-8213/ab960f](https://doi.org/10.3847/2041-8213/ab960f)
- . 2021, *ApJL*, 913, L7, doi: [10.3847/2041-8213/abe949](https://doi.org/10.3847/2041-8213/abe949)
- Abbott, R., Abbott, T. D., Acernese, F., et al. 2023a, *Physical Review X*, 13, 011048, doi: [10.1103/PhysRevX.13.011048](https://doi.org/10.1103/PhysRevX.13.011048)
- . 2023b, *Physical Review X*, 13, 041039, doi: [10.1103/PhysRevX.13.041039](https://doi.org/10.1103/PhysRevX.13.041039)
- Acernese, F., Agathos, M., Agatsuma, K., et al. 2015, *Classical and Quantum Gravity*, 32, 024001, doi: [10.1088/0264-9381/32/2/024001](https://doi.org/10.1088/0264-9381/32/2/024001)
- Ali-Haïmoud, Y., Kovetz, E. D., & Kamionkowski, M. 2017, *PhRvD*, 96, 123523, doi: [10.1103/PhysRevD.96.123523](https://doi.org/10.1103/PhysRevD.96.123523)
- Amaro-Seoane, P., Audley, H., Babak, S., et al. 2017, arXiv e-prints, arXiv:1702.00786, doi: [10.48550/arXiv.1702.00786](https://doi.org/10.48550/arXiv.1702.00786)
- Amaro-Seoane, P., Andrews, J., Arca Sedda, M., et al. 2023, *Living Reviews in Relativity*, 26, 2, doi: [10.1007/s41114-022-00041-y](https://doi.org/10.1007/s41114-022-00041-y)
- Antonini, F., Romero-Shaw, I., Callister, T., et al. 2025a, arXiv e-prints, arXiv:2509.04637, doi: [10.48550/arXiv.2509.04637](https://doi.org/10.48550/arXiv.2509.04637)
- Antonini, F., Romero-Shaw, I. M., & Callister, T. 2025b, *PhRvL*, 134, 011401, doi: [10.1103/PhysRevLett.134.011401](https://doi.org/10.1103/PhysRevLett.134.011401)
- Ashton, G., Hübner, M., Lasky, P. D., et al. 2019, *Bilby: Bayesian inference library*, *Astrophysics Source Code Library*, record ascl:1901.011. <http://ascl.net/1901.011>
- Aso, Y., Michimura, Y., Somiya, K., et al. 2013, *PhRvD*, 88, 043007, doi: [10.1103/PhysRevD.88.043007](https://doi.org/10.1103/PhysRevD.88.043007)
- Banagiri, S., Thrane, E., & Lasky, P. D. 2025, arXiv e-prints, arXiv:2509.15646, doi: [10.48550/arXiv.2509.15646](https://doi.org/10.48550/arXiv.2509.15646)
- Barkat, Z., Rakavy, G., & Sack, N. 1967, *PhRvL*, 18, 379, doi: [10.1103/PhysRevLett.18.379](https://doi.org/10.1103/PhysRevLett.18.379)
- Bartos, I., & Haiman, Z. 2025, arXiv e-prints, arXiv:2508.08558, doi: [10.48550/arXiv.2508.08558](https://doi.org/10.48550/arXiv.2508.08558)
- Baumgarte, T. W., & Shapiro, S. L. 2025, *PhRvL*, 135, 191401, doi: [10.1103/26yd-1mhd](https://doi.org/10.1103/26yd-1mhd)
- Bavera, S. S., Fragos, T., Qin, Y., et al. 2020, *A&A*, 635, A97, doi: [10.1051/0004-6361/201936204](https://doi.org/10.1051/0004-6361/201936204)
- Broekgaarden, F. S., Stevenson, S., & Thrane, E. 2022, *ApJ*, 938, 45, doi: [10.3847/1538-4357/ac8879](https://doi.org/10.3847/1538-4357/ac8879)
- Buchner, J. 2016, *PyMultiNest: Python interface for MultiNest*, *Astrophysics Source Code Library*, record ascl:1606.005. <http://ascl.net/1606.005>
- Chiba, T., & Yokoyama, S. 2017, *Progress of Theoretical and Experimental Physics*, 2017, 083E01, doi: [10.1093/ptep/ptx087](https://doi.org/10.1093/ptep/ptx087)
- Collaboration, L. S., Collaboration, T. V., & Collaboration, T. K. 2025, *GWTC-4.0: Population Properties of Merging Compact Binaries*, *Zenodo*, doi: [10.5281/zenodo.16911563](https://doi.org/10.5281/zenodo.16911563)
- Croon, D., Sakstein, J., & Gerosa, D. 2025, arXiv e-prints, arXiv:2508.10088, doi: [10.48550/arXiv.2508.10088](https://doi.org/10.48550/arXiv.2508.10088)
- De Luca, V., Desjacques, V., Franciolini, G., & Riotto, A. 2020, *JCAP*, 2020, 028, doi: [10.1088/1475-7516/2020/11/028](https://doi.org/10.1088/1475-7516/2020/11/028)
- De Luca, V., Franciolini, G., & Riotto, A. 2025, arXiv e-prints, arXiv:2508.09965, doi: [10.48550/arXiv.2508.09965](https://doi.org/10.48550/arXiv.2508.09965)
- Edelman, B., Doctor, Z., Godfrey, J., & Farr, B. 2022, *ApJ*, 924, 101, doi: [10.3847/1538-4357/ac3667](https://doi.org/10.3847/1538-4357/ac3667)
- Ezquiaga, J. M., & Holz, D. E. 2021, *ApJL*, 909, L23, doi: [10.3847/2041-8213/abe638](https://doi.org/10.3847/2041-8213/abe638)
- . 2022, *PhRvL*, 129, 061102, doi: [10.1103/PhysRevLett.129.061102](https://doi.org/10.1103/PhysRevLett.129.061102)
- Farmer, R., Renzo, M., de Mink, S. E., Fishbach, M., & Justham, S. 2020, *ApJL*, 902, L36, doi: [10.3847/2041-8213/abbadd](https://doi.org/10.3847/2041-8213/abbadd)
- Farmer, R., Renzo, M., de Mink, S. E., Marchant, P., & Justham, S. 2019, *ApJ*, 887, 53, doi: [10.3847/1538-4357/ab518b](https://doi.org/10.3847/1538-4357/ab518b)
- Farr, W. M., Fishbach, M., Ye, J., & Holz, D. E. 2019, *ApJL*, 883, L42, doi: [10.3847/2041-8213/ab4284](https://doi.org/10.3847/2041-8213/ab4284)
- Fishbach, M., Essick, R., & Holz, D. E. 2020, *ApJL*, 899, L8, doi: [10.3847/2041-8213/aba7b6](https://doi.org/10.3847/2041-8213/aba7b6)
- Fishbach, M., Holz, D. E., & Farr, B. 2017, *ApJL*, 840, L24, doi: [10.3847/2041-8213/aa7045](https://doi.org/10.3847/2041-8213/aa7045)

- Fowler, W. A., & Hoyle, F. 1964, *ApJS*, 9, 201, doi: [10.1086/190103](https://doi.org/10.1086/190103)
- Fuller, J., & Ma, L. 2019, *ApJL*, 881, L1, doi: [10.3847/2041-8213/ab339b](https://doi.org/10.3847/2041-8213/ab339b)
- Gerosa, D., & Berti, E. 2017, *PhRvD*, 95, 124046, doi: [10.1103/PhysRevD.95.124046](https://doi.org/10.1103/PhysRevD.95.124046)
- Gerosa, D., & Fishbach, M. 2021, *Nature Astronomy*, 5, 749, doi: [10.1038/s41550-021-01398-w](https://doi.org/10.1038/s41550-021-01398-w)
- Gottlieb, O., Metzger, B. D., Issa, D., et al. 2025, *ApJL*, 993, L54, doi: [10.3847/2041-8213/ae0d81](https://doi.org/10.3847/2041-8213/ae0d81)
- Goyal, S., Villarrubia-Rojo, H., & Zumalacarregui, M. 2025, arXiv e-prints, arXiv:2512.17631, doi: [10.48550/arXiv.2512.17631](https://doi.org/10.48550/arXiv.2512.17631)
- Guo, W.-H., Li, Y.-J., Wang, Y.-Z., et al. 2024, *ApJ*, 975, 54, doi: [10.3847/1538-4357/ad758a](https://doi.org/10.3847/1538-4357/ad758a)
- Guttman, N., Payne, E., Lasky, P. D., & Thrane, E. 2026, *ApJ*, 996, 144, doi: [10.3847/1538-4357/ae17af](https://doi.org/10.3847/1538-4357/ae17af)
- Harshe, R., Prasad, R., & Ajith, P. 2026, arXiv e-prints, arXiv:2604.14247, doi: [10.48550/arXiv.2604.14247](https://doi.org/10.48550/arXiv.2604.14247)
- Hu, Q., Narola, H., Heynen, J., et al. 2025, arXiv e-prints, arXiv:2512.17550, doi: [10.48550/arXiv.2512.17550](https://doi.org/10.48550/arXiv.2512.17550)
- Hu, W.-R., & Wu, Y.-L. 2017, *National Science Review*, 4, 685, doi: [10.1093/nsr/nwx116](https://doi.org/10.1093/nsr/nwx116)
- King, A. R., & Dehnen, W. 2005, *MNRAS*, 357, 275, doi: [10.1111/j.1365-2966.2005.08634.x](https://doi.org/10.1111/j.1365-2966.2005.08634.x)
- Kıroğlu, F., Kremer, K., & Rasio, F. A. 2025, *ApJL*, 994, L37, doi: [10.3847/2041-8213/ae1eeb](https://doi.org/10.3847/2041-8213/ae1eeb)
- Li, E.-K., Liu, S., Torres-Orjuela, A., et al. 2025a, *Reports on Progress in Physics*, 88, 056901, doi: [10.1088/1361-6633/adc9be](https://doi.org/10.1088/1361-6633/adc9be)
- Li, G.-P., & Fan, X.-L. 2025, arXiv e-prints, arXiv:2509.08298, doi: [10.48550/arXiv.2509.08298](https://doi.org/10.48550/arXiv.2509.08298)
- Li, Y.-J., Tang, S.-P., Gao, S.-J., Wu, D.-C., & Wang, Y.-Z. 2024a, *ApJ*, 977, 67, doi: [10.3847/1538-4357/ad83b5](https://doi.org/10.3847/1538-4357/ad83b5)
- Li, Y.-J., Tang, S.-P., Wang, Y.-Z., & Fan, Y.-Z. 2024b, *ApJ*, 976, 153, doi: [10.3847/1538-4357/ad888b](https://doi.org/10.3847/1538-4357/ad888b)
- Li, Y.-J., Tang, S.-P., Xue, L.-Q., & Fan, Y.-Z. 2025b, arXiv e-prints, arXiv:2507.17551, doi: [10.48550/arXiv.2507.17551](https://doi.org/10.48550/arXiv.2507.17551)
- Li, Y.-J., Wang, Y.-Z., Tang, S.-P., Chen, T., & Fan, Y.-Z. 2025c, *ApJ*, 987, 65, doi: [10.3847/1538-4357/add535](https://doi.org/10.3847/1538-4357/add535)
- Li, Y.-J., Wang, Y.-Z., Tang, S.-P., & Fan, Y.-Z. 2024c, *PhRvL*, 133, 051401, doi: [10.1103/PhysRevLett.133.051401](https://doi.org/10.1103/PhysRevLett.133.051401)
- . 2025d, arXiv e-prints, arXiv:2509.23897, doi: [10.48550/arXiv.2509.23897](https://doi.org/10.48550/arXiv.2509.23897)
- LIGO Scientific Collaboration, Aasi, J., Abbott, B. P., et al. 2015, *Classical and Quantum Gravity*, 32, 074001, doi: [10.1088/0264-9381/32/7/074001](https://doi.org/10.1088/0264-9381/32/7/074001)
- Luo, J., Chen, L.-S., Duan, H.-Z., et al. 2016, *Classical and Quantum Gravity*, 33, 035010, doi: [10.1088/0264-9381/33/3/035010](https://doi.org/10.1088/0264-9381/33/3/035010)
- Mandel, I., & Farmer, A. 2022, *PhR*, 955, 1, doi: [10.1016/j.physrep.2022.01.003](https://doi.org/10.1016/j.physrep.2022.01.003)
- Mandel, I., Farr, W. M., & Gair, J. R. 2019, *MNRAS*, 486, 1086, doi: [10.1093/mnras/stz896](https://doi.org/10.1093/mnras/stz896)
- Mapelli, M., Spera, M., Montanari, E., et al. 2020, *ApJ*, 888, 76, doi: [10.3847/1538-4357/ab584d](https://doi.org/10.3847/1538-4357/ab584d)
- Marchant, P., Langer, N., Podsiadlowski, P., Tauris, T. M., & Moriya, T. J. 2016, *A&A*, 588, A50, doi: [10.1051/0004-6361/201628133](https://doi.org/10.1051/0004-6361/201628133)
- Miller, M. C., & Colbert, E. J. M. 2004, *International Journal of Modern Physics D*, 13, 1, doi: [10.1142/S0218271804004426](https://doi.org/10.1142/S0218271804004426)
- Moore, C. J., Gerosa, D., & Klein, A. 2019, *MNRAS*, 488, L94, doi: [10.1093/mnrasl/slz104](https://doi.org/10.1093/mnrasl/slz104)
- Paiella, L., Ugolini, C., Spera, M., Branchesi, M., & Arca Sedda, M. 2025, *ApJL*, 994, L54, doi: [10.3847/2041-8213/ae1447](https://doi.org/10.3847/2041-8213/ae1447)
- Passenger, L., Banagiri, S., Thrane, E., et al. 2025, arXiv e-prints, arXiv:2510.14363, doi: [10.48550/arXiv.2510.14363](https://doi.org/10.48550/arXiv.2510.14363)
- Plunkett, C., Callister, T., Zevin, M., & Vitale, S. 2026, arXiv e-prints, arXiv:2601.07908, doi: [10.48550/arXiv.2601.07908](https://doi.org/10.48550/arXiv.2601.07908)
- Popa, S. A., & de Mink, S. E. 2025a, *ApJL*, 995, L76, doi: [10.3847/2041-8213/ae20f1](https://doi.org/10.3847/2041-8213/ae20f1)
- . 2025b, arXiv e-prints, arXiv:2509.00154, doi: [10.48550/arXiv.2509.00154](https://doi.org/10.48550/arXiv.2509.00154)
- Qin, Y., Fragos, T., Meynet, G., et al. 2018, *A&A*, 616, A28, doi: [10.1051/0004-6361/201832839](https://doi.org/10.1051/0004-6361/201832839)
- Ray, A., & Kalogera, V. 2025, arXiv e-prints, arXiv:2510.18867, doi: [10.48550/arXiv.2510.18867](https://doi.org/10.48550/arXiv.2510.18867)
- Renzo, M., Cantiello, M., Metzger, B. D., & Jiang, Y.-F. 2020, *ApJL*, 904, L13, doi: [10.3847/2041-8213/abc6a6](https://doi.org/10.3847/2041-8213/abc6a6)
- Sesana, A. 2016, *PhRvL*, 116, 231102, doi: [10.1103/PhysRevLett.116.231102](https://doi.org/10.1103/PhysRevLett.116.231102)
- Shao, Y., & Li, X.-D. 2022, *ApJ*, 930, 26, doi: [10.3847/1538-4357/ac61da](https://doi.org/10.3847/1538-4357/ac61da)
- Stegmann, J., Olejak, A., & de Mink, S. E. 2025a, *ApJL*, 992, L26, doi: [10.3847/2041-8213/ae0e5f](https://doi.org/10.3847/2041-8213/ae0e5f)
- . 2025b, arXiv e-prints, arXiv:2507.15967, doi: [10.48550/arXiv.2507.15967](https://doi.org/10.48550/arXiv.2507.15967)
- Talbot, C., & Golomb, J. 2023, *MNRAS*, 526, 3495, doi: [10.1093/mnras/stad2968](https://doi.org/10.1093/mnras/stad2968)
- Tang, S.-P., Wang, H.-T., Li, Y.-J., & Fan, Y.-Z. 2026, *Science Bulletin*, 71, 83, doi: [10.1016/j.scib.2025.11.002](https://doi.org/10.1016/j.scib.2025.11.002)

- The LIGO Scientific Collaboration, the Virgo Collaboration, & the KAGRA Collaboration. 2025a, arXiv e-prints, arXiv:2507.08219, doi: [10.48550/arXiv.2507.08219](https://doi.org/10.48550/arXiv.2507.08219)
- The LIGO Scientific Collaboration, the Virgo Collaboration, the KAGRA Collaboration, et al. 2025b, arXiv e-prints, arXiv:2508.18083, doi: [10.48550/arXiv.2508.18083](https://doi.org/10.48550/arXiv.2508.18083)
- Tong, H., Callister, T. A., Fishbach, M., et al. 2025a, arXiv e-prints, arXiv:2511.05316, doi: [10.48550/arXiv.2511.05316](https://doi.org/10.48550/arXiv.2511.05316)
- Tong, H., Fishbach, M., Thrane, E., et al. 2025b, arXiv e-prints, arXiv:2509.04151, doi: [10.48550/arXiv.2509.04151](https://doi.org/10.48550/arXiv.2509.04151)
- Vaccaro, M. P., Mapelli, M., Périgois, C., et al. 2024, *A&A*, 685, A51, doi: [10.1051/0004-6361/202348509](https://doi.org/10.1051/0004-6361/202348509)
- Wang, H.-T., Tang, S.-P., Li, P.-C., & Fan, Y.-Z. 2025a, arXiv e-prints, arXiv:2509.02047, doi: [10.48550/arXiv.2509.02047](https://doi.org/10.48550/arXiv.2509.02047)
- Wang, Y.-Z., Li, Y.-J., Gao, S.-J., Tang, S.-P., & Fan, Y.-Z. 2025b, arXiv e-prints, arXiv:2510.22698, doi: [10.48550/arXiv.2510.22698](https://doi.org/10.48550/arXiv.2510.22698)
- Wang, Y.-Z., Li, Y.-J., Vink, J. S., et al. 2022, *ApJL*, 941, L39, doi: [10.3847/2041-8213/aca89f](https://doi.org/10.3847/2041-8213/aca89f)
- Wang, Y.-Z., Tang, S.-P., Liang, Y.-F., et al. 2021, *ApJ*, 913, 42, doi: [10.3847/1538-4357/abf5df](https://doi.org/10.3847/1538-4357/abf5df)
- Wang, Z.-Y., Qin, Y., Hu, R.-C., et al. 2026, *A&A*, 708, A62, doi: [10.1051/0004-6361/202557224](https://doi.org/10.1051/0004-6361/202557224)
- Woosley, S. E. 2017, *ApJ*, 836, 244, doi: [10.3847/1538-4357/836/2/244](https://doi.org/10.3847/1538-4357/836/2/244)
- Woosley, S. E., & Heger, A. 2021, *ApJL*, 912, L31, doi: [10.3847/2041-8213/abf2c4](https://doi.org/10.3847/2041-8213/abf2c4)
- Yang, Q., You, Z.-Q., & Fan, X. 2025, arXiv e-prints, arXiv:2512.20890, doi: [10.48550/arXiv.2512.20890](https://doi.org/10.48550/arXiv.2512.20890)
- You, Z.-Q., Zhu, X.-J., Ashton, G., Thrane, E., & Zhu, Z.-H. 2021, *ApJ*, 908, 215, doi: [10.3847/1538-4357/abd4d4](https://doi.org/10.3847/1538-4357/abd4d4)
- Yuan, C., Chen, Z.-C., & Liu, L. 2025, arXiv e-prints, arXiv:2507.15701, doi: [10.48550/arXiv.2507.15701](https://doi.org/10.48550/arXiv.2507.15701)